Title Page

Time Course of Dual-task Interference in the Brain in Simulated Driving Environment

Seyed Reza Hashemirad[1], Maryam Vaziri-Pashkam[2], Mojtaba Abbaszadeh[3]*

[1] School of Cognitive Sciences, Institute for Research in Fundamental Sciences (IPM), Tehran, Iran

[2] Department of Psychological and Brain Sciences, University of Delaware, Newark, DE, USA

[3] Department of Neurosciences, Université de Montréal, Montréal, QC, Canada

***Corresponding author and lead contact:**

Mojtaba Abbaszadeh,

Department of Neurosciences,

Université de Montréal

Montréal, QC CANADA H3T 1J4 21

Email: abbaszadeh989@gmail.com

Abstract

Due to the brain's limited cognitive capacity, simultaneous execution of multiple tasks can lead to performance impairments, especially when the tasks occur closely in time. This limitation is known as dual-task interference. We aimed to investigate the time course of this phenomenon in the brain, utilizing a combination of EEG, multivariate pattern analysis (MVPA), and drift diffusion modeling (DDM). In a simulated driving environment, participants first performed a tone discrimination task, followed by a lane-change task with varying onset time differences (Stimulus Onset Asynchrony, SOA), either short or long. As expected, the dual-task interference resulted in an increase in lane-change reaction time. The DDM analysis indicated that this increase was attributable to changes in both the decision time and the post-decision time. Our MVPA findings revealed a decrease in decoding accuracy of the lane-change task from ~200 to ~800 ms after stimulus onset in short SOA compared to long SOA, suggesting a change in lane-change direction information in both decision and motor processing stages. Moreover, a distinct pattern of generalization emerged in temporal generalization of short SOA condition, coupled with a delayed latency from ~500 ms in conditional generalization. Searchlight analysis illustrated the progression of this information reduction, starting in occipital, parietal, and parieto-occipital leads responsible for visual response and decision making, and then transferring to the frontal leads for mapping decisions onto motor regions. Consistent with the hybrid dual-task theory, our results suggest that processing of the two tasks occurs in partial parallel until the decision bound is reached. After the decision is made, another competition arises between the two tasks in motor areas for execution. Overall, our findings shed light on

the intricate mechanisms underlying dual-task interference and provide further insights into the simultaneous processing of multiple tasks in the brain.

Keywords: Dual-task interference, Driving, Electroencephalogram (EEG), Multivariate analysis (MVPA), Drift diffusion modeling (DDM)

Introduction

In the fast-paced modern world, the act of multitasking while driving has become increasingly prevalent. With the widespread adoption of smartphones and in-vehicle technology, drivers frequently find themselves juggling multiple activities while operating a vehicle. However, the consequences of engaging in secondary tasks on driving performance have raised significant concerns regarding road safety. Extensive scientific research has explored this topic, illuminating the negative impact of multitasking on driving abilities (Abbas-Zadeh, Hossein-Zadeh, & Vaziri-Pashkam, 2021; Levy, Pashler, & Boer, 2006; Strayer & Johnston, 2001; Welford, 1952). One important aspect to consider is the time course of dual-task interference during driving. In other words, it is crucial to determine when exactly the interference occurs and how long it lasts. To address this question, we conducted a study using the combination of Electroencephalogram (EEG), Multivariate Pattern Analysis (MVPA) and Drift Diffusion Modeling (DDM) in a well-controlled simulated driving environment.

Previous EEG studies on dual-task interference have predominantly relied on univariate methods to explore the neural correlations of dual task interference (Dell'Acqua, Jolicoeur, Vespignani, & Toffanin, 2005; Matthews, Garry, Martin, & Summers, 2006; Pratt, Willoughby, & Swick, 2011; Sigman & Dehaene, 2008; Töllner, Strobach, Schubert, & Mueller, 2012). These methods have focused on analyzing either the peak or the time course of Event-Related Potentials (ERPs). However, these findings do not clarify whether the observed brain activity changes are a result of general factors like task difficulty, attentional variations, and mental effort, or if they are specifically due to interference in processing of the tasks. An effective method to address this constraint is

to explore the information over time for each task individually across the entire brain using multivariate pattern analysis (MVPA) during dual-task performance (King & Dehaene, 2014; Marti, King, & Dehaene, 2015; Rajaei, Mohsenzadeh, Ebrahimpour, & Khaligh-Razavi, 2019). By adopting MVPA, researchers gain the ability to explore the temporal progression of information processing in the brain while dual-task interference occurs. For instance, this method enables the decoding of specific features related to a driving task (e.g., detecting the direction of a turn or lane change) based on the pattern of responses across brain sensors. Changes in decoding accuracy during dual-task interference can then be measured to assess alterations in the information content at different time points.

Current theories of the dual-task paradigm typically acknowledge three stages of processing for each task: perceptual, central, and motor processing (Hibberd, Jamson, & Carsten, 2013; Pashler & Johnston, 1989; Sternberg, 1969). However, there is an ongoing debate about the dynamics of these processing stages during dual-task situations. In the literature, two main theories attempt to explain this dynamic: the bottleneck theory and the central capacity-sharing theory. The bottleneck theory suggests that when two tasks occur closely together, the central processing of the second task is delayed until the central stage of the first task is completed. However, the perceptual and motor stages can occur in parallel (McCann & Johnston, 1992; Pashler, 1994; Pashler & Johnston, 1989; Ruthruff, Pashler, & Klaassen, 2001; Sigman & Dehaene, 2005, 2006; M. N. Tombu et al., 2011). On the other hand, the central capacity-sharing theory proposes that the central stages of both tasks can be processed in parallel, with the limited cognitive resources shared between the tasks in a graded

manner. This theory also rules out interference during the perceptual and motor stages (Duncan, 1980; Huestegge & Koch, 2010; Mike Tombu & Jolicœur, 2002; Michael Tombu & Jolicœur, 2003). The core disagreement between these theories revolves around the central stage or the decision related stage. The serial bottleneck theory posits a strict sequential processing of tasks, while the capacity-sharing theory suggests that the central stage can handle multiple tasks concurrently, but with the challenge of allocating limited resources, which can potentially lead to interference.

Using drift diffusion modeling (DDM), a framework for modeling the distinct processing stages involved in two-choice tasks (Gold & Shadlen, 2007; Ratcliff, Smith, Brown, & McKoon, 2016; Shadlen & Newsome, 2001), recent research has indicated that the dynamics of dual-task interference cannot be fully explained by either of the bottleneck and central capacity-sharing theories alone (Abbas-Zadeh et al., 2021; Zylberberg, Ouellette, Sigman, & Roelfsema, 2012). As a result, hybrid theories of dual-task processing have been put forward (Abbas-Zadeh et al., 2021; Zylberberg et al., 2012). According to the hybrid theory, the central stages of both tasks may be processed in a partial-parallel manner, but a bottleneck exists when routing the decision to motor structures. This means that not only the central processing stages are affected by dual-task demands, but the interference also extends into the motor stages. While these theories have mainly relied on behavioral data, the integration of EEG and MVPA offers an opportunity to test them using neural data, providing a more comprehensive understanding of dual-task processing and interference.

Marti et al. (2015) applied the MVPA method of time decomposition to MEG data. They discovered a more complicated dynamic for the interference and showed that brain

processes could operate in parallel for the first 500 milliseconds but beyond that the two tasks repel each other. They suggested that the two tasks compete for the attentional resources and as a result processing of the first task is shortened while processing of the second task is either lengthened or postponed. Both the central capacity-sharing and bottleneck theories cannot explain their findings. However, the hybrid theory might be more optimal to explain the dual-task interference based on their findings. In Marti et al. (2015) study, they trained a decoder to distinguish between the non-interfering dual-task condition and the distractor condition. The key distinguishing factor between these two conditions was the presence or absence of motor execution. In other words, their decoder primarily discriminated based on the motor execution factor, diminishing the impact of task-specific information over time. To address this limitation, our approach involves training a decoder specifically to discriminate between the two main conditions of each task in both single- and dual-task conditions. This allows us to investigate how dual-task interference influences the information processing of each task individually across time.

To date, most experimental designs exploring dual-task interference have predominantly focused on simple tasks like visual discrimination (e.g., distinguishing objects, colors, or orientations) or tone discrimination tasks (e.g., identifying high and low pitches). However, the gap between these artificial tasks and real-world scenarios, such as driving, is substantial. In real-life situations, individuals frequently encounter more intricate and sequential motor movements that involve multiple steps, which contrasts with the simplicity of artificial tasks typically limited to a single step. Additionally, the priority assigned to different tasks differs significantly. In artificial

experiments, neither task inherently outweighs the other in importance. Conversely, in real-world driving, the act itself holds a significantly higher priority, thereby diminishing the significance of the second task, even if presented first. Moreover, real-world environments involve continuous tasks like driving, exposing individuals to a multitude of distractions. In contrast, most artificial tasks consist of discrete and isolated stimuli. To approach the complexities of real-life dual-task situations more closely, we developed a dual-task paradigm within a simulated driving environment (Abbas-Zadeh et al., 2021; Abbaszadeh, Hossein-Zadeh, Seyed-Allaei, & Vaziri-Pashkam, 2023). By considering these critical factors, we aimed to bridge the gap towards real-world conditions, thereby enhancing the practicality and relevance of our research.

Here, we used a dual-task paradigm in which a tone discrimination task was followed by a lane-change task either immediately (100ms later, short Stimulus Onset Asynchrony, SOA) or after a longer gap (600ms later, long SOA). Using MVPA and EEG, we investigated the temporal dynamic of information about the driving lane-change direction in single- and dual-task conditions. We fitted a drift diffusion model on the behavioral data to estimate the time course of the central or decision stage of the lane-change task and compare it to the subsequent MVPA results. Additionally, we used searchlight analysis to localize multivariate effects and determine the time-course of each electrode classification accuracy and to examine which electrodes are most important for the classification accuracy at each time step. Together the results of MVPA and DDM and their relationship can provide useful information about the time course of dual-task interference and provide evidence for or against models of dual task interference.

Results

Behavioral results

The mean reaction time and accuracy was compared between the short, the long SOA and single task conditions in each task (Figure 1B). Reaction times for the lane-change task were 782 ± 71, 541 ± 84 and 605 ± 53 for short SOA, long SOA and single lane-change conditions, respectively. As was predicted by the psychological refractory period, there was a significant effect of condition on reaction time of the lane-change task ($F(2,36) = 168.4$, $p < 0.0001$). Subsequent post-hoc analysis using Tukey HSD revealed that the short SOA had significantly longer reaction time in comparison to both the long SOA ($p < 0.0001$) and the single lane-change ($p < 0.0001$) conditions. Furthermore, a significantly shorter reaction time was observed in the long SOA condition compared to the single lane-change condition ($p < 0.001$). This difference in reaction time may be attributed to the priming effect of the tone task in the long SOA condition, which was not presented in the single lane-change condition.

The lane-change task accuracy was 93 ± 1 %, 97 ± 0.8 % and 96 ± 1% for short SOA, long SOA and single lane-change conditions, respectively (Figure 1C). Analysis of lane-change task accuracy revealed a significant difference among conditions ($F(2,36) = 142.31$, $p < 0.0001$). Participants had also significantly higher driving accuracy in the long SOA ($p<0.0001$) and single drive ($p < 0.0001$) conditions in comparison to the short SOA condition, however there was no significant difference between accuracies of the single lane-change and the long SOA conditions ($p = 0.51$). The average lane-change accuracy was more than 90% in all three conditions.

Tone task reaction times were 800 ± 123, 825 ± 99 and 827 ± 103 for the short SOA, the long SOA and the single tone conditions, respectively (Figure 1B). There was no significant effect between reaction time of the tone task conditions ($F(2,36) = 1.23$, $p = 0.3$) that was always presented first. On the other hand, there was a significant difference between conditions for the tone accuracy ($F(2,36) = 50.07$, $p < 0.001$). Accuracies for the tone task were 93 ± 2 %, 97 ± 1 % and 98 ± 0.9 % for the short SOA, the long SOA, and the single tone conditions, respectively (Figure 1C). The short SOA's tone accuracy significantly dropped in comparison to the long SOA ($p < 0.0001$) and the single tone condition ($p < 0.0001$). The long SOA had also significantly lower accuracy in comparison to the single tone condition ($p = 0.02$).

These findings, consistent with our previous studies (Abbas-Zadeh et al., 2021; Abbaszadeh et al., 2023), are in agreement with the previous reports of dual-task interference, in that, performing two tasks in close succession significantly impairs the reaction time of the second task and the accuracy of both tasks while the reaction time of the first task remains unaffected. Furthermore, significantly lower reaction time of the long SOA in comparison to the single lane-change reveals the priming effect of the tone task in which the tone works as a cue to draw attentional resources to the expected lane-change task.

Drift Diffusion Model

To better understand the effect of dual-task interference on the time course of each stage of the processing of the lane-change task (accumulation time and motor execution), a drift diffusion model (DDM) was fitted to the behavioral RTs of the lane-

change task. DDM assumes that participants accumulate information continuously until sufficient evidence is gathered in favor of one of the choices (one of two thresholds is hit, Figure 1D)

For each participant, first, outliers were removed, then for each condition four parameters were considered (mean and standard deviation of the delayed onset or pre accumulation time, drift rate and post accumulation time). The boundaries, sigma and starting point were considered equal across conditions. Subsequently, RTs of all conditions were pooled together and fitting procedure was done only once for each subject by the maximum likelihood method using the BADS algorithm in MATLAB. Finally, one-way repeated measures ANOVA was used to infer significance. The estimated parameters and R^2 for each participant are summarized in supplementary table 1-3. The model was fit for each participant separately and the average R^2 was > 0.99 for all three conditions (Figure 1F).

The mean estimated parameters are shown in Figure 1E. The mean drift rate during the accumulation time was 3.38±1, 4.25±1 and 4.18±1 for the short SOA, the long SOA and the single task conditions, respectively. There was a significant effect of condition on drift rate ($F(2,36) = 15.54$, $p < 0.0001$). Subsequent Tukey's HSD post-hoc analysis revealed that both the long SOA and the single lane-change condition had significantly higher drift rate compared to the short SOA (ps < 0.001), however there was no significant difference between the long SOA and the single lane-change condition ($p = 0.9$). The mean pre accumulation time was 172 ± 37, 84 ± 37 and 88 ± 43 for the short SOA, the long SOA and the single condition, respectively. There was also a significant effect of condition on the pre accumulation time mean ($F(2,36) = 38.7$, $p < 0.0001$).

Consistent with drift rate results, both the long SOA and the single task had a lower pre accumulation time than the short SOA (ps < 0.0001) while there was no significant difference between the long SOA and the single lane-change (p = 0.9). This may be due to the divided attention at the beginning of the task that could delay the pre accumulation time for the short SOA. Moreover, the same effect was evident in standard deviation (std) of cumulative gaussian in the model. There was a significant effect of task condition on standard deviation ($F(2,36) = 18.8$, $p < 0.0001$). Likewise, both the long SOA and the single lane-change had lower std than the short SOA (long: $p = 0.001$; single: $p < 0.001$) implying a quick rise of drift rate whereas the short SOA's drift rate increased slowly. There was also no significant difference between the long SOA and the single lane-change in std ($p = 0.88$).

Finally, post accumulation time estimated by the model was 451 ± 45, 242 ± 47 and 300 ± 56 ms for the short SOA, the long SOA and the single lane-change conditions, respectively. There was a significant effect of task condition on post accumulation time ($F(2,36) = 128$, $p < 0.0001$). In post-hoc analysis, once again both the long SOA and the single lane-change had significantly shorter post accumulation time than the short SOA (ps < 0.0001); however contrary to the previous parameters, the long SOA had significantly shorter post accumulation time than the single lane-change ($p < 0.001$), which suggests that the potential priming effect of tone on the lane change response in the long SOA condition, mainly affected the post accumulation time resulting in shorter reaction times.

Altogether, the DDM results suggest that not only were the drift rate or evidence accumulation time affected by the dual-task performance but also the interference

resulted in delayed onset of evidence accumulation and longer post accumulation times. Hence, these results are in agreement with hybrid models that both decision and non-decision times are affected as two tasks get closer in time.

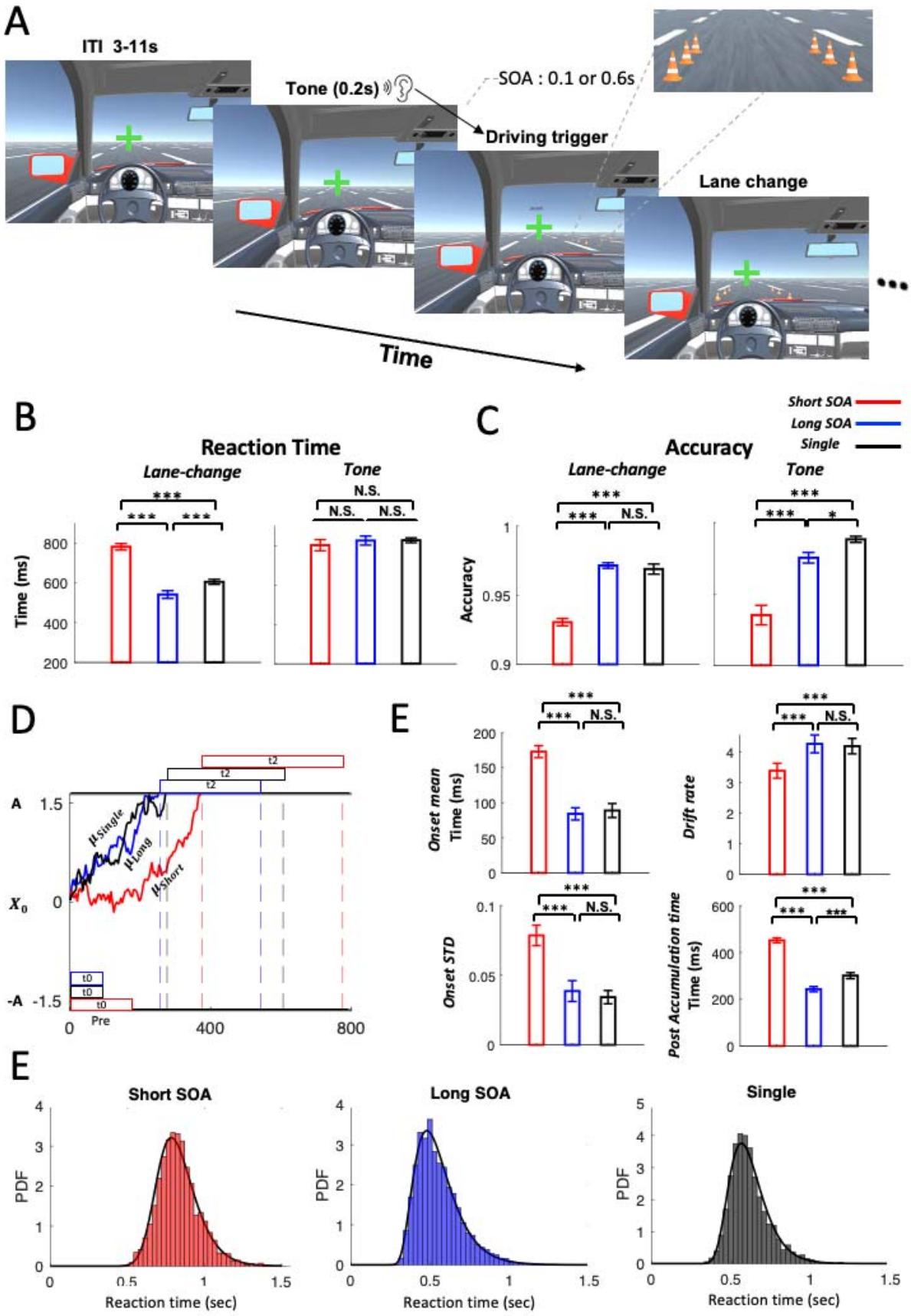

Figure 1. Paradigm, behavioral and DDM results. A) Dual-task paradigm: The sequence of events for one sample trial. First, the tone task was presented and lasted for 200 ms, then the cones were presented with 100 or 600 ms delay (either long or short SOA) after the tone onset. The inter-trial interval (ITI) varied between 1 to 3 sec. Participants were instructed to respond to the tone task first and then to perform the lane-change as fast as possible. B) Reaction times (RT) both tasks. The left and right panels show the lane-change RT and tone RT, respectively, for the short SOA (red) and long SOA (blue) and single task (black) conditions. The error bars represent standard error of mean (SEM, * $p < 0.05$, ** $p < 0.01$, *** $p < 0.001$). C) the same format as B but for the accuracy of both tasks. D) Schematic of drift-diffusion modeling based on estimated parameters by the model. A and X_0 are the boundary and the starting point and μ is the drift rate. t_0 is the estimated onset of cumulative gaussian that discounts early samples, and t_2 is the post accumulation time. Subjects accumulate evidence continuously until one of the decision boundaries is reached. Note, the reduction in drift rate coupled with increased post accumulation time in short SOA that favors the hybrid model. E) Estimated parameters of the DDM for the lane-change task. Drift rate, Onset, STD and post accumulation times are presented, for the long SOA (blue), the short SOA (red) and single task condition (black). E) RT distribution of each condition for lane-change task and the estimated PDF by the model (solid line). The distribution of the lane-change task RT for the three conditions, for the participants (histogram) and the model (black lines). Bin width is 40 ms. The fraction of variance explained by the model fits (R^2) were 0.99 for all three conditions.

Multivariate analysis

Multivariate pattern analysis (MVPA) was applied to EEG data to characterize representational dynamics of the dual-task interference. Applying this method to each task separately allows for a fine-resolution observe at the temporal dynamics of the information for each task and how each task is influenced by the dual-task interference.

For each participant and task, MVPA was employed using Support Vector Machine (SVM) classifiers to analyze the data. The objective was to investigate potential differences in how information about lane-change direction conditions (right vs. left) and tone frequency discrimination (high vs. low) was encoded across conditions over time.

Then, we generated temporal and conditional generalization matrices by employing the trained SVM at any given time to other time bins and conditions, respectively.

Lane-change task decoding accuracy significantly decreased in the short SOA

Figure 2 illustrates the decoding accuracy of the lane-change task, both time-locked to the onset of the lane-change stimulus (Figure 2A) and time-locked to the lane-change reaction time (Figure 2B) for various task conditions. To identify time-points with significantly above chance decoding accuracy, we employed a right-sided Wilcoxon signed-rank test with FDR correction, setting alpha to 0.05. We compared the earliest time that the decoding accuracy was above chance to determine the decoding onset latency across conditions. As depicted in Figure 2A, the average decoding onset latency was 236 ± 180, 196 ± 56, and 164 ± 120 ms (mean ± std resampling) for short SOA, long SOA and single-task conditions, respectively. There was a significant effect of condition on onset between conditions ($F(2,198) = 51.8$, $P < 0.0001$). In subsequent post-hoc analysis, the single lane-change condition had significantly earlier onset latency compared to both the short and the long SOA conditions (ps < 0.001). Moreover, the long SOA onset latency was also earlier than the short SOA ($p < 0.0001$). Decoding accuracy was then followed by rapid increase reaching its first maximum peak accuracy in 264 ± 78 ms, 229 ± 56 ms and 242 ± 64 ms for the short SOA, the long SOA and the single lane-change conditions respectively, yet there was no significant effect of condition on the difference between peak latency of either of the conditions ($F(2,34) = 3.1$, $P = 0.07$, Greenhouse-Geisser corrected).

Subsequently, pairwise two-sided Wilcoxon signed-rank test was used to assess differences in decoding accuracy of the lane-change task conditions. The first period of difference in accuracies of the long SOA versus the short SOA started from 228 ms after stimulus onset and it remained significant until 252 ms ($Zs > 2.3$, $ps < 0.05$). This was followed by a brief period from 432 ms to 468 ms ($Zs > 2.76$, $ps < 0.028$) and again around long SOA reaction time from 496 ms to 680 ms ($Zs > 2.5$, $ps < 0.04$). The next significant decoding accuracy periods were related to reaction time of the lane-change in the short SOA condition from 984 ms 1024 ms and from 1104 to 1124 ($Zs > 2.5$, $ps < 0.04$). Furthermore, there was no significant difference in the accuracy of the long SOA vs the single lane-change condition. The short SOA vs single condition comprised of brief periods of significance: First a very brief period from 228 ms to 240 ms ($Zs > 2.5$, $ps < 0.05$), followed by segregated periods from 524 ms to 604 ms before single drive reaction time ($Zs > 2.7$, $ps < 0.03$) and finally from 636 ms to 780 ms associated to single drive reaction time ($Zs > 2.7$, $ps < 0.03$).

As shown in Figure 2B, there was also a reduction in short SOA's decoding accuracy compared to long SOA from ~ 128 to 40 ms ($Zs > 2.76$, $ps < 0.048$) prior to the reaction time and a very brief period from ~20 to 10 ms ($Zs > 3.2$, $ps < 0.035$) compared to single condition in reaction time-locked decoding accuracy. This reduction in decoding accuracy right before the reaction time once again exhibited an interference during motor processing and execution stages.

On the other hand, there was no significant decoding accuracy in neither of the long, short SOA and single conditions nor their differences for the firstly presented tone task (Figure S1). One potential explanation for this apparent drop in accuracy might be

attributed to the saliency of the lane change task that imposes a great intrinsic priority level and draws attentional resources which makes the tone task less important even if it is presented first. Additionally, another factor to consider is the relatively minor frequency difference between the two tone conditions, as compared to the pronounced left/right shift required for the lane change task.

Taken together, the significant reduction in the decoding accuracy in the short vs the long SOA (and even a brief period in the short SOA vs the single lane-change), particularly from 220 to 250 ms is in contradiction with the pure bottleneck theory. This theory hypothesizes that when two tasks occur in close succession central processing of the second task is delayed until after the central stage of the first task. As a result, decoding accuracy of neither of the tasks should be affected as they are happening in serial; hence, this theory cannot explain the drop in decoding accuracy of the lane-change task in short SOA. On the other hand, the capacity sharing model doesn't predict any limitation after the decision has been made which is in contrast with our results. In both the long SOA and single lane-change conditions, a notable difference was observed in the period before their respective reaction times, as compared to the short SOA. These findings clearly indicate a certain level of limitation and competition occurring after the central processing stage, which aligns with the predictions of the hybrid theory.

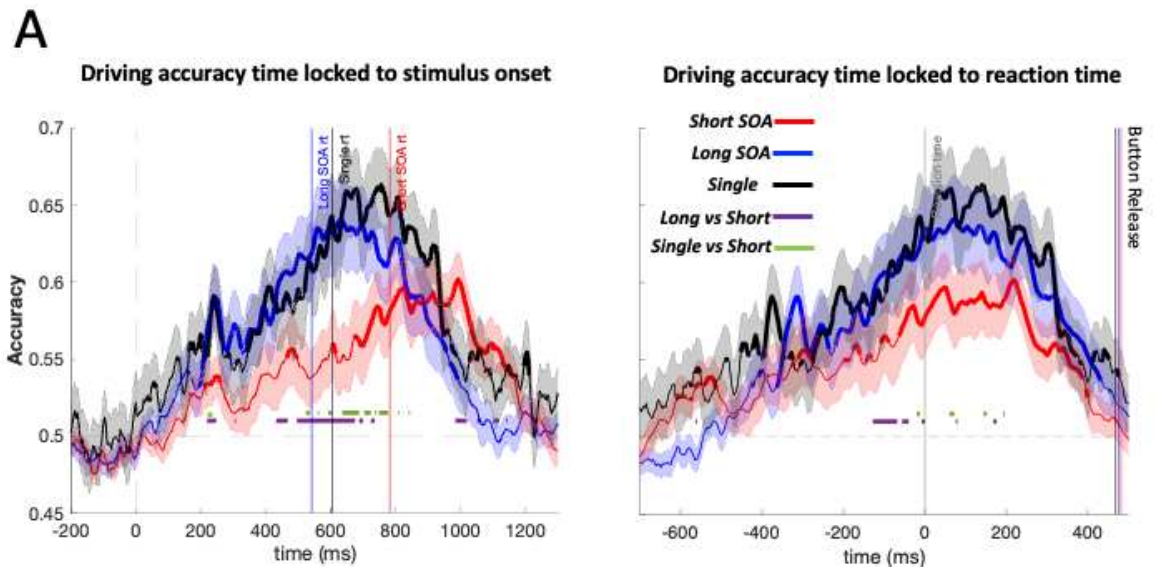

Fig 2. Temporal dynamics of dual task interference in lane-change task. A) Multivariate pattern analysis of EEG data. Time courses of decoding accuracies for the long, the short SOA and the single lane-change condition averaged across 18 subjects time-locked to the stimulus onset (left) and the reaction time (right). lane-change onset is shown by dashed vertical lines. The chance level decoding accuracy is shown by the vertical dashed line at 0.5. Three vertical lines are the corresponding reaction times of long, short SOA and single drive conditions, respectively. Thicker lines indicate a decoding accuracy significantly above chance (right-sided signed-rank test, FDR corrected across time, $p < 0.05$), shaded error bars represent standard error of the mean (SEM). Ticker horizontal lines represent significant differences between long and short SOA (purple) and single drive and short SOA (green). There was no significant difference between the long SOA and the single drive decoding accuracy throughout the epoch. The legends indicate corresponding reaction times and accuracies of each condition. For display purposes, data was smoothed using a moving average with five sample points.

Short SOA has different pattern of generalization in comparison to long SOA in lane-change task

To evaluate how dual-task interference may affect temporal generalization of each condition, time-time decoding matrices were created for each condition of each task. To construct the time-time decoding matrices, a SVM classifier trained at any time was tested on its discrimination performance at all other times of the given epoch. Temporal generalization provides helpful information about how different stages of brain processes evolve and interact across time.

The temporal generalization was influenced by the various task conditions of the lane-change task (Fig. 3A). The overall time-time decoding matrix in the long SOA represented two distinct patterns of generalizations. First, a diagonal-shaped generalization (cascade of processing happening one after the other with some overlap) from ~0-250 ms after stimulus onset, suggesting the perceptual and central stage processing happening in a partially overlapping cascade. This was followed by a square-shaped pattern (sustained-activity pattern) of generalization representing a sustained activity that started ~250 ms before reaction time until ~500 ms after it. This sustained activity is reasonable after the first button press reaction time as the participants should hold the key and maintain the car position between the cones. Since there was no interference in the long SOA, completely distinct patterns of generalization emerged.

Similar pattern was also evident in the time-time decoding matrix of the single lane-change condition, however a wider generalization pattern at the beginning was

noticeable compared to the long SOA. Furthermore, the two generalization patterns were not as distinct as they were for the long SOA condition. In other words, as the priming effect of the long SOA seems draw more attentional resources to one task, the two patterns of generalization become more automatic and distinct. As a result, transferring information from central to motor areas happens quicker and smoother.

One striking aspect of Figure 3A is the distinct off diagonal generalization (the significant generalization in upper left and lower right of the square) in the long SOA and the single lane-change conditions. This pattern emerged in classifiers trained ~200-500 ms and tested 900-1300 ms (and vice versa) in the long SOA and classifiers trained ~0-600 ms and tested 1000-1300 ms (and vice versa) in the single lane-change condition, suggesting brain activities related to information processing of both conditions were reactivated once the task was completed.

For the short SOA, significantly above-chance decoding performance started right after stimulus onset followed by a diagonal generalization pattern until ~350 ms. Notably, the information was passed on to another diagonal-shaped pattern of information processing through a weak transitional state. This stage was not evident in neither the long SOA nor the single lane-change and started from ~350 ms to ~650 ms. It is probably indicative of interference in motor areas in that, once the decision is made since two motor actions should be executed in close succession, strong interference emerges. Beyond ~700ms, time-time decoding matrix represents a square shaped generalization proposing a sustained activity from 700ms throughout the given time epoch.

Contrary to the long SOA and the single lane-change, the distinct off-diagonal generalization after the task completion was rather weak in the short SOA condition. It was noticeable in classifiers trained 200-500 ms and tested in 1100-1300 ms (and vice versa), suggesting that information processing of the early stages was reactivated (King & Dehaene, 2014).

The tone task decoding performance was substantially compromised by a more salient the lane-change task. Statistical analysis revealed no significant decoding performance between neither of conditions.

The statistical comparison of the differences in temporal generalization between lane-change conditions was performed by calculating the onset, offset, and duration of accuracy above change level of classifiers at each time bin by resampling method (see methods). The single lane-change condition was considered as the baseline condition, and both other conditions were compared with the baseline for onset, offset and duration parameters (Figure 3B).

The classifiers trained with the long SOA exhibited a significantly earlier onset at approximately 124 ± 41 to 196 ± 57 ms ($Zs > 2.9$, $ps < 0.004$) after stimulus onset compared to the single lane-change condition. Subsequently, there was a delayed onset observed in classifiers trained at approximately 212 ± 8 to 480 ± 74 ms ($Zs > 2.1$, $ps < 0.04$), with no significant differences between the conditions until approximately 700 ms. Moreover, the long SOA once again showed an earlier onset in classifiers trained at approximately 708 ± 71 to 1064 ± 72 ms ($Zs > 2.07$, $ps < 0.049$), and at approximately 1148 ± 22 to 1300 ± 32 ms ($Zs > 2.1$, $ps < 0.04$).

Regarding the short SOA condition compared to the single lane-change condition, classifiers trained from approximately 240 ± 10 ms to 300 ± 20 ms exhibited a brief period of delayed onset for the short SOA ($Zs > 2.3$, $ps < 0.02$). Subsequently, there were no significant differences between the short SOA and lane-change conditions until 600 ms, at which point there was another delayed onset from approximately 600 ± 58 ms to 1148 ± 308 ms ($Zs > 2.15$, $ps < 0.04$). However, in classifiers trained from 1152 ± 301 ms to 1300 ± 4 ms, the short SOA showed an earlier onset ($Zs > 4.6$, $ps < 0.0001$).

Moreover, the long SOA condition also exhibited a delayed onset compared to the short SOA in classifiers trained from approximately 212 ± 21 ms to 496 ± 90 ms ($Zs > 2.39$, $ps < 0.02$). Subsequently, there was an earlier onset in classifiers trained from approximately 648 ± 71 ms to 1124 ± 34 ms ($Zs > 2.23$, $ps < 0.03$), followed by another delayed onset until 1246 ± 5 ms ($Zs > 2.23$, $ps < 0.03$).

Regarding the offset latency, the long SOA exhibited a significantly earlier offset in classifiers trained from ~0 to 200 ms compared to both the single lane-change and the short SOA ($Zs > 2.12$, $ps < 0.047$). Subsequently, there was a delay in offset latency from ~200 ± 18 to 296 ± 177 ms and 344 ± 178 to 400 ± 204 ms compared to the single lane-change ($Zs > 2.12$, $ps < 0.046$) and a delay at ~220 ± 43 to 600 ± 61 ms compared to the short SOA ($Zs > 2.2$, $ps < 0.03$). In classifiers trained at ~600 to 1000 ms, the long SOA had an intermediate offset latency, being delayed compared to the single lane-change but earlier compared to the short SOA ($Zs > 2.16$, $ps < 0.043$). Beyond 1000 ms, there was no significant difference in offset latency between the long SOA, single lane-change, and short SOA conditions. For the short SOA, classifiers exhibited an earlier offset, from ~220 ± 11 to 546 ± 56 ms after stimulus onset, compared to the

single lane-change (Zs > 2.13, ps < 0.046). This was followed by a significant delayed offset of ~600 ± 105 to 1060 ± 74 ms (Zs > 2.1, ps < 0.044), beyond which time there was no difference in offset latency between the conditions.

Moreover, the significant differences in onset and offset latencies between the long SOA lane-change condition resulted in shorter durations for classifiers trained from 0 ± 42 to 200 ± 63 ms compared to the single lane-change condition (Zs > 2.2, ps < 0.034). This observation is likely attributed to the priming effect, which directs attentional resources to the second task, facilitating quicker and smoother processing. Additionally, classifiers trained from ~200 ± 65 to 250 ± 27 and ~ 400 to 500 ms exhibited significantly longer durations compared to the single condition (Zs > 2.01, ps < 0.05), suggesting that the sustained activity occurred earlier for the long SOA. Subsequent longer significant periods included classifiers trained at 600 ± 154 to 1100 ± 21 ms and 1200 ± 39 to 1300 ± 32 ms (Zs > 2.08, ps < 0.047), which were related to the sustained activity of motor activation.

In case of the short SOA, classifiers trained from 200 ± 74 to 548 ± 100 displayed a significantly shorter duration compared to the single lane-change condition (Zs > 3.21, ps < 0.001). This finding is likely due to the fact that the single condition transferred information to execution areas without interruption, resulting in an earlier sustained activity with longer duration. In contrast, the short SOA exhibited delays, which postponed motor execution. Additionally, there was a longer duration from 600 ± 154 to 720 ± 168 ms (Zs > 3.44, ps < 0.0001) followed by another shorter duration from 836 ± 143 to 1136 ± 222 (Zs > 2.17, ps < 0.035) ms in time of motor execution.

Comparing the long and short SOA durations, the short SOA showed considerably longer durations in classifiers trained from ~30 ± 62 to 180 ± 75 ms ($Zs > 2.79$, $ps < 0.006$). This was followed by a significantly shorter duration in classifiers trained from ~185 ± 57 to 600 ± 257 ms ($Zs > 2.15$, $ps < 0.038$), in short SOA, exhibiting a pattern similar to the single condition. Subsequently, another period of shorter duration in the short SOA, ranging from ~750 ± 106 to 1050 ± 131 ms, was related to motor execution ($Zs > 1.97$, $ps < 0.05$). This was followed by a longer duration period from ~1148 ± 177 to 1250 ± 7 ms ($Zs > 2.23$, $ps < 0.031$).

These results emphasize the shorter duration and quicker processing of the long SOA during evidence accumulation time of DDM analysis compared to both the short SOA and the single condition, leading to a faster transition to motor areas for execution. Notably, the striking aspect of temporal generalization was an additional diagonal generalization pattern in the short SOA, evident by an earlier offset and shorter duration from ~300-600 ms, while the long SOA and the single condition exhibited sustained generalization of motor execution.

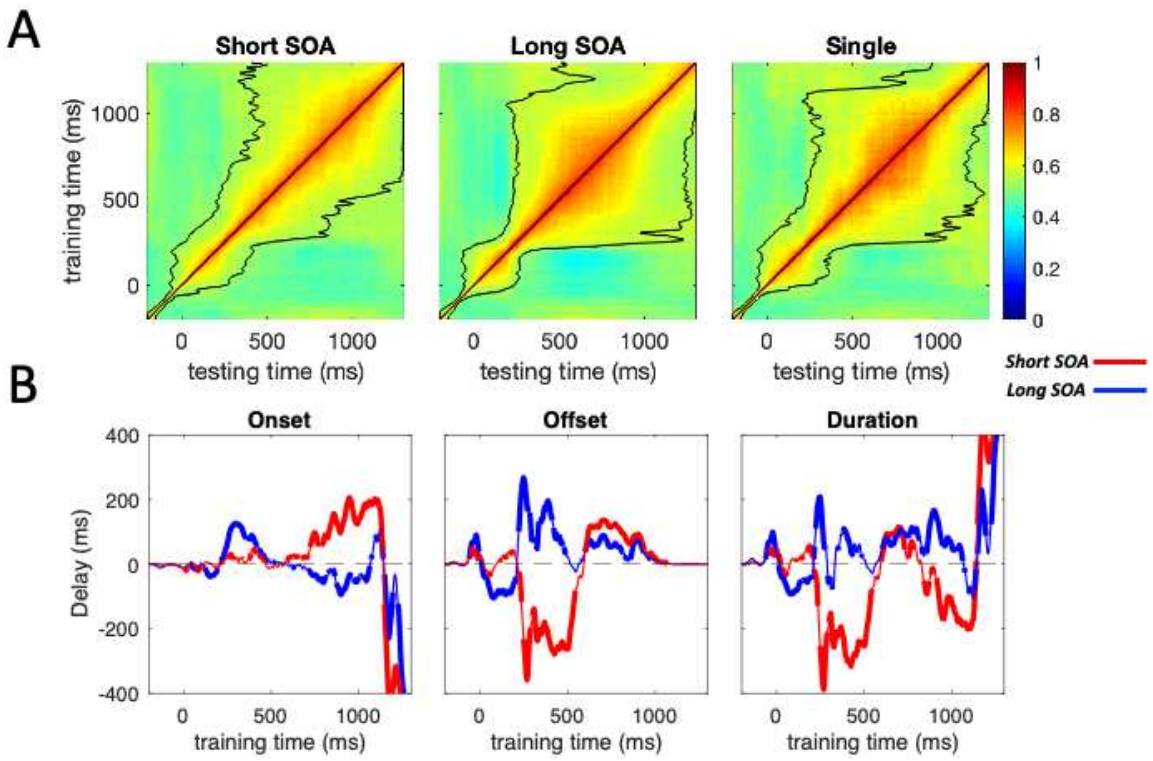

Figure 3. Temporal generalization patterns for the lane-change task. A) Time-time decoding matrices of the long SOA, the short SOA, and the single lane-change task. A classifier trained at any given time is also tested at all other time points resulting in a training time x testing time temporal generalization matrix for each condition. Horizontal axis indicates testing times, and the vertical axis indicates training times. Color bars represent percent of decoding AUC (chancel level = 50%); Within each time-time decoding matrix, onset and offset latencies are shown by solid black lines and smoothed by moving average of five samples. **B)** Parameters of temporal generalization for the lane-change task. Onset latency was defined as the earliest time where performance became significantly above chance (i.e., AUC=0.5) for at least 5 consecutive time bins (20 milliseconds). offset latency was defined the same as the earliest time when decoding performance was insignificant for 20 milliseconds. The standard deviation was computed by a resampling method. The duration was defined as the time between onset and offset latencies. Colored lines represent the mean difference between the single lane-change (horizontal dash line) and both the long (blue) and the short (red) SOAs. Positive and negative values indicate earlier and delayed onset and offset latencies and longer and shorter duration periods, respectively. Thicker lines represent a significant (two-sided signed-rank test, FDR corrected across time, $p < 0.05$) difference from the single lane-change

condition. For display purposes, data was smoothed using a moving average with five sample points.

Conditional generalization reveals a delay in the short SOA processes

To construct conditional generalization matrices, we employed classifiers trained in one condition and tested their performance in other conditions. This approach allowed us to investigate whether the observed temporal generalization differences between conditions were linked to a higher signal-to-noise ratio in the long SOA and single conditions, or if they revealed distinct patterns of generalization and information processing speed (Rajaei et al., 2019). The overall generalization displayed a narrow period of significance with a delayed onset and earlier offset (Figure 4A). This phenomenon might be attributed to varying time courses of processing in different generalizations, which potentially affected decoding performance in test conditions. To ensure a reliable comparison across conditions, we focused solely on peak latency in the analysis (Figure 4B).

The short train/long test and short train/single test matrices exhibited a narrow generalization pattern, displaying a delayed onset and an earlier offset throughout the time course of generalization (Figure 4A, top row). Comparatively, the peak latency occurred earlier in classifiers trained from 700 ± 41 to 1150 ± 233 ms for the short train/long test condition ($Zs > 3.5$, $ps < 0.001$), and from 750 ± 67 to 1150 ± 224 ms for the short train/single test condition ($Zs > 3.1$, $ps < 0.004$, Figure 4B, top panel). Consequently, the generalization was shifted towards the upper diagonal areas.

The time-time decoding matrix, trained in the long SOA condition and tested in the short SOA (long train/short test) exhibited a delayed pattern of generalization (Figure 4A,

middle row). The long train/short test matrix demonstrated narrow generalization, with a delayed onset and earlier offset in most cases. Notably, the peak latency was significantly delayed in classifiers trained from 444 ± 200 to 870 ± 68 ms ($Zs > 3.6$, $ps < 0.0001$), leading to a shifted generalization pattern below the diagonal (Figure 4B, middle panel). Similarly, the long train/single test also displayed a delayed peak latency in classifiers from ~348 ± 118 to 790 ± 45 ms but to a lower extent ($Zs > 3.6$, $ps < 0.0001$) followed by an earlier latency from ~ 800 to 900 ms ($Zs > 3.6$, $ps < 0.0001$, Figure 4B, middle).

Furthermore, the same generalization pattern was observed in the single train condition (Figure 4A, bottom row). The single train/short test matrix exhibited a narrow generalization pattern with a delayed peak latency in classifiers trained from ~560 ± 130 to 890 ± 41 ms ($Zs > 3.2$, $ps < 0.003$) compared to the single train/single test condition (Figure 4B, button panel). This delay in the peak latency is likely related to the motor execution process, causing the generalization matrix to shift below the diagonal. In the single train/long test matrix, an earlier peak latency was observed in classifiers trained from 650 ± 24 to 960 ± 125 ms ($Zs > 3.2$, $ps < 0.003$), corresponding to the time of motor execution (Figure 4B, button panel). These conditional generalization results align with those of Marti et al. (2015) indicating a delay in the short SOA after ~500 ms during motor processing.

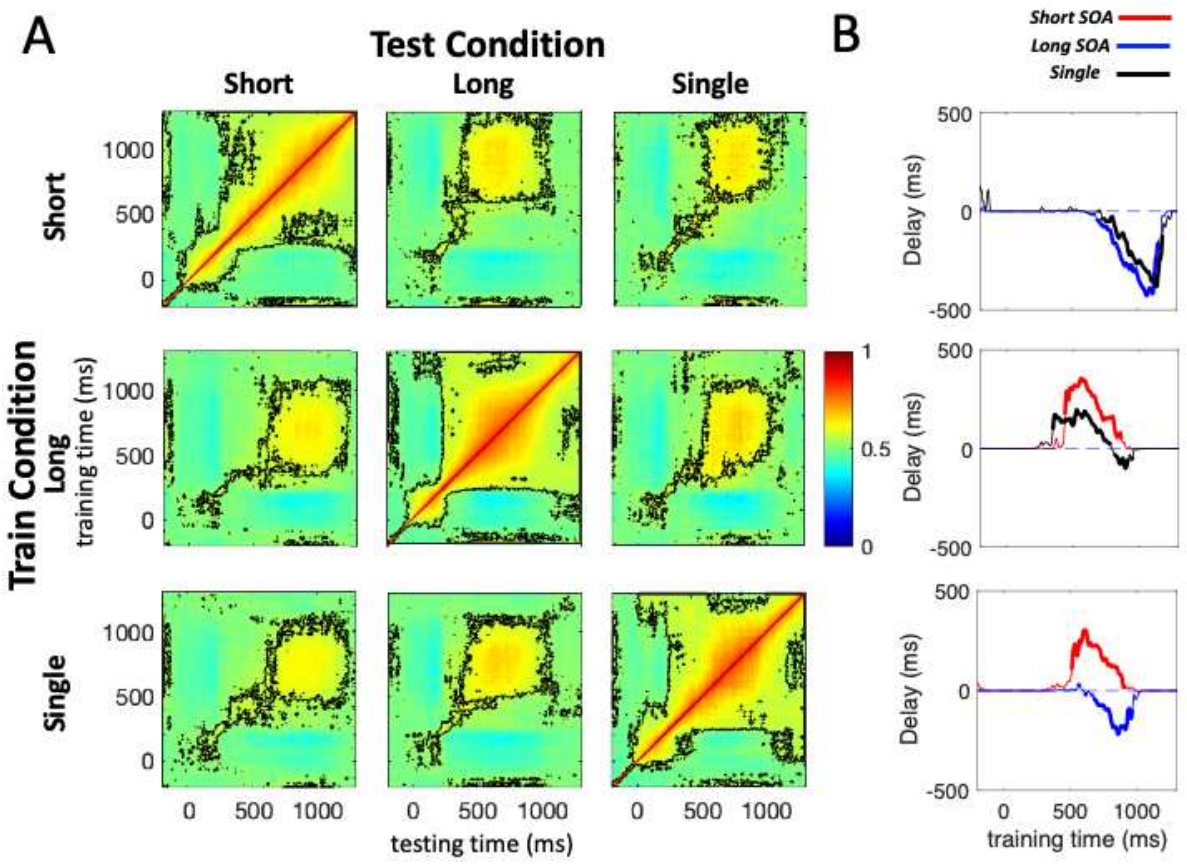

Figure 4. Conditional generalization of the lane-change task. A) Conditional generalization matrices. The classifiers were trained on one condition and were then tested to discriminate right shift vs left shift in other conditions. Significantly above chance decoding performance are shown by dashed contour lines (right-sided signed-rank test, FDR-corrected across time, $p<0.05$). In each figure the horizontal axis indicates testing times and the vertical axis indicates training times. Each row represents classifiers trained by one condition and columns are the tested conditions. Color bars represent percent of decoding AUC (chancel level = 50%); **B)** Peak latency parameter of conditional generalization matrix. Peak latency was considered as the time point where accuracy is maximum. In each row the condition for which train and test conditions were identical e.g, the long SOA train and the long SOA test is represented as the horizontal dashed line and the resulting peak latency of other two conditions were compared to the horizontal line. Thicker lines represent a significant (two-sided signed-rank test, FDR corrected across time, $p < 0.05$) difference from the dashed line (zero delay).

Searchlight analysis disclosed the topographical flow of information processing

To identify the most informative EEG electrodes related to the lane-change task, the searchlight analysis was conducted. This analysis is a useful approach to localize multivariate effects. For each channel and its neighbors decoding was done using a sliding window of 50 ms as a feature matrix with steps of 4 ms. Consistent with predictions, at the beginning of the trial, parietal and occipital regions were more involved in classification performance and as the time elapsed the information was gradually transferred to the frontal lobe for the response selection and the motor execution. The decoding performance is shown in Figure 5 for the short SOA, the long SOA, and the single lane-change conditions in steps of 200 ms.

In short SOA, performances decreased throughout the trial. In 200 ms, only few electrodes in right centro-parietal (‘CP4’, ’CP6’), frontal electrodes ('F3', 'F4', 'F5', 'F7', ’AF7’), ‘FC5’, ‘TP8,10’ had significant decoding performance ($Zs > 2.3$, $ps < 0.049$). Notably the maximum decoding was in left lateral frontal electrodes ($Zs > 2.55$, $ps < 0.03$) and decoding performance among parietal and occipital electrodes was compromised by the interference compared to the long SOA. At 400 ms, only frontal electrodes ('AF7', 'F3', 'F5', 'F6’, 'F7') had significant performance ($Zs > 2.3$, $ps < 0.049$). This is the time that a distinct diagonal generalization (~300-600 ms) emerged in the temporal generalization matrix. Since the frontal electrodes had higher decoding performance; the frontal region is probably the area for competition of two tasks for motor execution. In 600 ms frontal electrodes’ performance remained significant ('AF3', 'AF7', 'F1', 'F3', 'F5'). Moreover, fronto-central ('FC4'), fronto-parietal ('FP1'), central ('C4'), centro-parietal ('CP5'), parietal ('P7') and temporo-parietal ('TP7', 'TP9') had also significant performance ($Zs > 2.3$, $ps < 0.049$). At the time of reaction time in 800 and

1000 ms frontal regions had higher decoding performance ('AF3', 'AF7', 'F1', 'F3', 'F4', 'F5', 'F6', 'F7', 'FC3', 'FC4', 'FC5', 'FC6', 'FT10', 'FT7', (Zs > 2.65, ps < 0.03). Moreover, parietal, central, centro-parietal and parieto-occipital electrodes also had significant performance ('C3', 'C4', 'C5', 'C6', 'CP3', 'CP4', 'CP6', 'P3', 'P7', 'PO3', 'PO7', (Zs > 2.3, ps < 0.049) indicating a high decoding accuracy and extensive processing at reaction time.

For the long SOA, at 200 ms after stimulus onset, parietal and occipital regions had higher decoding performance. All parietal and parieto-occipital electrodes' performance was significant. Moreover, 'O1', lateral central and centro-parietal ('C3' , C4', 'C5', 'C6', 'CP3' , 'CP4' , 'CP6'), lateral frontal and fronto-central ('AF8', 'F4', 'F5', 'F6', 'FC3', 'FC4', 'FC5', 'FC6'), temporal and temporo-parietal electrodes ('T7', 'T8', 'TP10', 'TP8') had significantly above chance performance (Zs > 2.39, ps < 0.042) with maximum decoding in parietal ('P4', 'P8', 'P6'), parieto-occipital ('PO4', 'PO8') and centro-parietal electrodes ('CP4', 'CP6', Zs > 2.7, ps < 0.025). After that in 400 ms, frontal electrodes had higher decoding performance indicating the preparation of information for execution. All frontal electrodes, lateral fronto-central ('FC3', 'FC4', 'FC5', 'FC6'), fronto-temporal ('FT10', 'FT7', 'FT8'), parietal ('P6', 'P7') and temporo-parietal ('TP7', 'TP10) had significant performance (Zs > 2.3, ps < 0.049), with maximum decoding in frontal ('F3', 'F5', 'F7') and fronto-central ('FC3', 'FC4', 'FC5', 'FC6') electrodes (Zs > 3.04, ps < 0.016). Likewise, in 600 and 800 ms the same frontal, lateral fronto-central, fronto-parietal ('FPz', 'FP1') and fronto-temporal ('FT10', 'FT7', 'FT8') electrodes had the highest performance (Zs > 2.36, ps < 0.045). Moreover, lateral central, all parietal and parieto-occipital electrodes, temporal and temporo-parietal electrodes ('T7', 'T8', 'TP10', 'TP7',

'TP9') had significantly above chance performance (Zs > 2.36, ps < 0.045). However, the performance gradually decreased since the trial was nearly completed and in 1000 ms few electrodes in lateral frontal ('AF7', 'F4', 'F5', 'F6', 'F7'), centro-parietal ('CP3', 'CP5'), 'FP2', 'FC3', 'TP7' and 'TP9' had significant performance (Zs > 2.35, ps < 0.046).

The single lane-change followed a similar long SOA decoding time-course but with reduced decoding performance. In 200 ms only a few electrodes in the right lateral centro-parietal ('CP4', 'CP6') had significantly above chance decoding (Zs > 2.25, ps < 0.05). Notably, in 400 ms centro-parietal ('CP3', 'CP5'), parietal ('P3', 'P5'), temporo-parietal ('TP10', 'TP7', 'TP9'), left lateral frontal ('F3', 'F5') and fronto-temporal ('FT10') had significant performance (Zs > 2.39, ps < 0.042), whereas in the long SOA, the information processing was most significant in frontal electrodes in time 400 ms. In 600 ms, frontal electrodes had higher performance. All frontal electrodes, lateral fronto-central ('FC3', 'FC4', 'FC5', 'FC6'), fronto-temporal ('FT10'), right lateral parietal ('P6', 'P8') and central ('C1', C4') electrodes had significantly above chance decoding performance (Zs > 2.36, ps < 0.045). In 800 ms the processing was more extensive as all frontal electrodes, lateral fronto-central ('FC3', 'FC4', 'FC5', 'FC6'), fronto-temporal ('FT10', 'FT7', 'FT8'), lateral central and centro-parietal ('C4', 'C5', 'CP3', 'CP4', 'CP6') had significant performance (Zs > 2.31, ps < 0.049) with maximum performance in left lateral frontal electrodes (Zs > 3.02, ps < 0.016). Once again in 1000 ms performance declined and only a few electrodes 'FC5', 'FCz' and 'FT7' had significant performance (Zs > 2.43, ps < 0.039).

Taken together, the topographical time-course clearly showed the pattern of information processing that begins in occipital, parietal, and parieto-occipital regions responsible for visual response and decision making and then transfers to the frontal region for mapping the decision on the motor regions. The decoding performance was significantly compromised in the short SOA. Moreover, the distinct generalization pattern at ~300-600 ms in the short SOA indicating interference, particularly in motor execution, occurred in frontal and fronto-central electrodes.

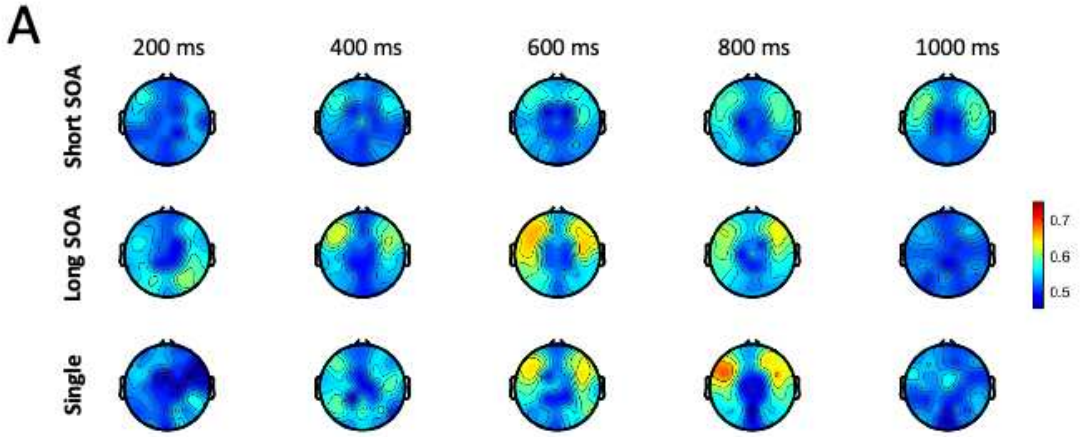

Figure 5. Searchlight analysis

Topographical plot of searchlight analysis for the short SOA (upper row), long SOA (middle row) and single lane-change condition (lower row) in steps of 200 ms. Searchlight analysis was done using a sliding window of 50 ms with 4 ms steps. In each window the decoding performance (AUC) of each electrode was calculated and the corresponding topographical map was plotted using EEGLAB 'topoplot' function.

Discussion

The goal of this study was to investigate the time course of processing the dual-task interference in the brain through the combination of EEG, multivariate pattern analysis (MVPA) and drift diffusion model (DDM). We aimed at testing different theories proposed to explain the dual-task paradigm mainly capacity sharing, bottleneck and hybrid models and to find a model that could best account for its dynamics. Our behavioral results, consistent with our previous studies (Abbas-Zadeh et al., 2021; Abbaszadeh et al., 2023), showed an increase in RT in the second task and a decrease in accuracy of both tone and lane-change task in the short SOA compared to the long SOA trials, confirming that the performance was influenced by the dual-task interference.

The peak decoding accuracy of the lane-change task in the short SOA was significantly reduced compared to both the single and the long SOA conditions. These results are not consistent with pure bottleneck theory which predicts the central processing resources can only be made available for one task at a time (McCann & Johnston, 1992; Ruthruff et al., 2001; Sigman & Dehaene, 2005, 2006; M. N. Tombu et al., 2011), on the contrary our data showed central stage processing of two tasks occurred concurrently but with reduced efficiency indicating a parallel processing. The same effect was also evident in the DDM results as the model predicted a reduced rate of evidence accumulation. Moreover, the results revealed a delayed onset in both DDM and onset latency of MVPA in the short SOA that implies interference emerges as soon as the second task begins that delayed the onset of evidence accumulation.

The results of temporal generalization matrices disclosed that complex tasks cannot simply be divided into three distinct steps of perceptual, central and motor processing

but it is a chain of overlapping processes (Marti et al., 2015). The generalization matrix in the short SOA condition revealed a different pattern compared to both the single and the long SOA. The difference in generalization pattern was regarding the late central processing and mainly post accumulation time in classifiers trained ~300 to 600 ms, after the decision was made in the motor processing stage (Figure 4A). The decoding accuracy of the MVPA also significantly dropped in the mentioned time. This period mainly points to the competition of two tasks for execution and in subsequent searchlight analysis frontal and fronto-central electrodes were more involved in decoding in this period. Once again, this result contradicted the conventional hypothesis that only the central stages can be affected by interference (Pashler & Johnston, 1989) and was in favor of hybrid theory (Abbas-Zadeh et al., 2021; Zylberberg et al., 2012) that a degree of interference was evident in all processing stages. These results are in line with previous studies of hybrid models. As mentioned before, Zylberberg et al. (2012) and Abbas-Zadeh et al. (2021) suggested a hybrid model for dual-task interference where the central stage of two tasks can be processed in parallel but there also exists an interference for routing the decision to motor structures that accounts for the remaining portion of the psychological refractory period. Marti et al. (2015) also proposed a parallel processing architecture for the first 500 ms that brain processes can operate in parallel but beyond 500 ms the two tasks repel each other. They compete for the attentional access and forms a bottleneck as a result the processing stages of the second task is delayed or lengthened and processes of the first task shortens. Consistent their study, our conditional generalization results revealed parallel processing for the first 500ms as there was no delay in the peak latency of either of the

results but a delay in the peak latency beyond ~500 ms for short SOA appeared (Figure 4B). Moreover, the short SOA had a distinct diagonal pattern of temporal generalization mainly in the post accumulation time from ~300 to 600 ms that also resulted in reduced decoding accuracy indicating another competition in the mentioned time in motor areas for execution.

The overall direction of our results highlights that competition for attentional resources emerges as soon as the second task processing begins. The processing of the two tasks occurs in parallel until the decision bound is reached. Once the decision is made, there is another competition between the two tasks in motor areas for execution. This is evident from the reduced decoding accuracy (Figure 3A) and the temporal generalization patterns (Figure 4A) in the post-accumulation period. During this competition, intrinsic priorities and external instructions play a role in determining which task should be responded to first, allowing the winner to gain access to motor areas first. As a result, the reaction time of the second task is delayed, leading to the observed delay in conditional generalization beyond ~500 ms.

In our study, we observed a significant drop in tone task decoding performance, approaching near-chance levels. The saliency of the lane-change task and its more complicated, multistep nature and simulated lane-change environment could have imposed a higher intrinsic priority level, drawing attentional resources away from the tone task, leading to interference, as evident in the MVPA results. These findings highlight the crucial role of saliency in dual-task interference. As mentioned earlier, when two tasks compete for attentional resources, the more salient task tends to attract more attention. Consequently, this significant difference in saliency resulted in a

substantial reduction in the tone task's decoding performance, leading to chance levels. Furthermore, when the more salient task is presented before others, it can capture a significant portion of attentional resources, giving rise to the attentional blink phenomenon (Marti, Sigman, & Dehaene, 2012; Raymond, Shapiro, & Arnell, 1992). This intriguing phenomenon merits exploration in future studies to gain a deeper understanding of its implications.

One interesting result obtained from the behavioral and MVPA data was the significantly shorter reaction time and post-accumulation time, a smoother temporal generalization matrix and quicker transfer of data to the motor cortex in the long SOA compared to the single lane-change condition. This indicates that once the tone task was presented, it worked as a cue for the lane-change task and deployed the attentional resources toward these brain activities, in turn, participants would be ready to better perform the task. This result can be extended to the real lane-change situations in which sounding an alarm could draw attentional resources toward the lane-change task and results in better performance and decreases the rate of accidents.

We are aware that a number of limitations could have influenced the results obtained. Firstly, the more salient lane-change task imposed a great intrinsic priority which results in significant reduction in decoding performance of tone task. Although the effect of dual task interference was present in our behavioral, DDM and MVPA analysis, this prevented us from examining thoroughly the whole dynamics of the first task. The second downside regarding our experiment design was the absence of other SOAs to get a better view of the trend of brain activities over time. However, a clear pattern emerged by comparing the two Long and short SOAs.

The use of MVPA analysis on the EEG data with great temporal resolution as well as their combination with the DDM allowed us to successfully decode the time course of the brain processes during dual-task interference. As a result, we have proposed a theory in which brain processes of two tasks occur in parallel to accumulate sensory evidence until a decision bound is reached. The relative saliency of two tasks and the order of presentation affects the rate of decision accumulation. Once the decision is made, there is another competition in motor areas for execution. Intrinsic priority, external instructions and previous sensory processing are among factors that influence which task to be responded first. Finally, further studies should be conducted to identify the decoding time course of each task in an evenly distributed attentional resources situation.

Materials and methods

Participants

The study involved human participants. Nineteen right-handed volunteers (9 females), 20-30 years old with normal or corrected-to-normal vision and no history of neurological or psychiatric disorders participated in the experiment. Additionally, all participants were not expert video game players, as defined by having less than 2 hours of video-game usage per week in the past year. Volunteers completed a consent form before participating in the experiment and were financially compensated after finishing the experiment. Experiments were approved by ethics committee at Institute for Research in Fundamental Sciences (IPM).

Stimuli and Procedure

The dual-task paradigm consisted of a tone discrimination task and a driving lane change task. Participants sat at 50 cm from a 22″ LG monitor with a refresh rate of 60 Hz and a resolution of 1920 × 1080 and responded to the tasks using a computer keyboard. The Unity 3D game engine was used to design the driving environment.

For the tone task, a single pure tone of either a high (800 Hz) or low (400 Hz) frequency was presented for 200 milliseconds. Participants pressed the “x” and “z” keys on the computer keyboard with the middle and index fingers of their left hand to determine whether the tone was a high frequency or a low frequency, respectively. To provide feedback, if participants responded incorrectly, the green fixation cross turned red.

The driving environment included a straight highway with infinite lanes on the two sides, without left/right turns or any hills and valleys. This was to equalize all trials in terms of visual appearance for the purpose of the experiment (Fig. 1A). The driving stimulus was composed of two rows of traffic cones with three cones in each row. In each trial, traffic cones were unexpectedly displayed on one side of the lanes, and the participants had to guide the vehicle to the lane with the cones and drive through them. The distance between the two rows of cones was such that the vehicle could easily drive through them without collisions. The cones were always presented in the lane immediately to the left or the right of the driving lane so that the participants had to change only one lane per trial. The lane change was performed gradually, and the participants had to hold the corresponding key to direct the vehicle in between the two rows of cones, and then release the key when the vehicle was in the correct situation. Any collision with the

cones would be registered as an error, in which case the green fixation cross would disappear to provide negative feedback. The driving started with a given initial speed which was kept constant. During the experiment, the participant moved to the right or left lanes by pressing the keys using the middle and index fingers of their right hand, respectively (Fig. 1A).

The experiment consisted of the dual-task and single-task conditions. In the dual-task trials, the two tasks were presented with either a short (100 ms) or long (600 ms) SOA. In the single-task trials either the lane-change or the tone task was presented alone. In all dual task trials, the tone task was presented first. There was a total of eight dual-task conditions: two SOAs (short and long) x two lane-change directions (shift right/shift left) x two tone conditions (low/high pitch); and four single-task conditions: two lane-change directions and two tone conditions. In the dual-task conditions the task presentation order was fixed so that the tone was always presented first, and the lane-change task was presented second. Each condition was repeated four times in each run resulting in a total of 48 trials in every run. Each trial lasted for 3s with an inter-trial interval varying from 1s to 3s. We used Optseq software (Dale, Greve, & Burock, 1999) for optimizing the presentation order of trials in each run. The participants completed 12 runs and each lasted 3.6 min (216 sec).

The participants were instructed to focus on the fixation cross at the center of the screen (Figure 1A) and first respond to tone then the lane-change task as fast as possible. The eye tracking device using an Eyelink 1000 plus program was used to track their eye movements and remove trials exhibiting distracting eye movements.

The trial onset was determined by the presentation time of the tone stimulus, while the trial end was defined as the moment the rear end of the car reached the end of the traffic cone set. The lane-change task performance was evaluated as the percentage of trials in which the participant correctly detected the lane-change direction and successfully passed through the cones without any collisions. On the other hand, the tone task performance was assessed based on the number of correct identifications made by the participants.

Before performing the main experiment, all participants performed one training run similar to the main experiments. If their performance was 80% or higher, they would proceed to the main experimental runs. All participants could reach this threshold.

Drift-diffusion model

Drift diffusion Model (DDM) is a model that can be used to infer a wide range of cognitive decision processes (Gold & Shadlen, 2007; Ratcliff et al., 2016; Shadlen & Newsome, 2001). DDM assumes that participants accumulate information continuously until sufficient evidence is gathered in favor of one of the choices (one of two thresholds is hit). The model uses the following partial differential equation (Shinn, Lam, & Murray, 2020):

$$dx = \mu(x, t, \dots)dt + \sigma(x, t, \dots)dW$$

in which $\mu(x, t)$ is the instantaneous drift rate (i.e., the rate of evidence accumulation), $\sigma\ (sigma)$ is the instantaneous noise and x_0 is the probability density function of the initial position (bias toward one of the decisions). The drift diffusion process terminates when x reaches a threshold A (Fig 1D).

Here a variant of drift diffusion model (Zylberberg et al., 2012) was used in which another parameter *G (t, μ onset, σ onset)* was introduced. G is a cumulative gaussian distribution that was used to model the delayed onset of evidence accumulation to discount early samples compared to later samples. The reason for introducing this parameter was to observe if there was any delay in accumulation of evidence due to divided attention at the beginning of the second task as the two tasks get closer in time.

$$dx = (\mu(x,t,\dots)G(t,\mu_{onset},\sigma_{onset}))dt + \sigma(x,t,\dots)dW$$

To solve DDM, Fokker-Planck equation, a partial differential equation using the probability density of the decision variable at position x and time t, was used as follows (Shinn et al., 2020; Sigman & Dehaene, 2005).

$$\frac{\partial}{\partial t}\,\rho(x,t,\dots) = -\frac{\partial}{\partial x}\left(\mu(x,t,\dots)G(t,\mu_{onset},\sigma_{onset})\rho(x,t,\dots)\right) + \frac{\partial^2}{\partial x^2}\left(\frac{\sigma^2(x,t,\dots)}{2}\rho(x,t,\dots)\right)$$

Subsequently the Fokker-Planck equation was approximated by discretization using the Crank-Nicolson method (Shinn et al., 2020).

$$\frac{P_j^n - P_j^{n-1}}{\Delta t} = 0.5\left(-\frac{(\mu.G(n,\mu_{onset},\sigma_{onset}).P)_{j+1}^{n-1} - (\mu.G(n,\mu_{onset},\sigma_{onset}).P)_{j-1}^{n-1}}{2\Delta x} + \frac{(DP)_{j+1}^{n-1} + (DP)_{j-1}^{n-1} - 2(DP)_j^{n-1}}{\Delta x^2}\right) + 0.5\left(-\frac{(\mu.G(n,\mu_{onset},\sigma_{onset}).P)_{j+1}^{n} - (\mu.G(n,\mu_{onset},\sigma_{onset}).P)_{j-1}^{n}}{2\Delta x} + \frac{(DP)_{j+1}^{n} + (DP)_{j-1}^{n} - 2(DP)_j^{n}}{\Delta x^2}\right)$$

Here, P_j^n is defined as the probability distribution at the jth space-grid and the nth time-grid and $D = \sigma^2/_2$ is the diffusion coefficient.

Taken together, for each condition (short SOA, long SOA and single lane-change) four parameters were defined. Two parameters for mean and standard deviation of *G* (cumulative gaussian), one for drift rate and another for post accumulation time. The boundaries (*A*), sigma (σ) and starting point (x_0) were considered equal among conditions.

Results of DDM can be highly affected by outliers (especially fast outliers). Due to positive skewness in the RT distribution, first, we log transformed the distribution for each condition to better remove fast outliers and then we used MATLAB (Mathworks, 2021a) function isoutlier (which defines an outlier when a value is more than three scaled median absolute deviations (MAD) away from the median) to remove all outliers (Voss, Voss, & Lerche, 2015). Subsequently, data of all three conditions were pooled together and mentioned parameters were fitted using maximum likelihood method. Bayesian adaptive direct search (BADS, (Acerbi & Ma, 2017)) in MATLAB was used as optimization algorithm. In other words, the fitting procedure was done for all three conditions simultaneously with a total of 15 parameters. Finally, R-squared was used to assess the goodness of fit of the model for each participant.

EEG acquisition

The EEG signal was recorded using a 64-channel electrode-cap with tin electrodes. The electro-cap was organized according to the international 10/20 system and connected to

a Bayamed reference amplifier. Impedance was reduced to less than 10kW for all electrodes by means of a mildly abrasive electrolyte paste. Data was sampled with a frequency of 250Hz. The reference electrode was positioned on the left mastoid. The ground electrode was placed 1 cm inferior to the Oz electrode.

EEG preprocessing

The EEG data was exported to EEGLAB 14b (Delorme & Makeig, 2004) in MATLAB for further preprocessing and analysis. Firstly, the data was re-referenced to an average reference and offline bandpass filtered between 1-40 Hz. The EEGLAB Cleanline method was then applied to eliminate line noise at 50 Hz and its subharmonics. To remove noisy channels, three automatic channel rejection methods of EEGLAB (spectrum, probability, and kurtosis with a z-score threshold of 5%) were utilized, and channels labeled as bad based on at least two methods were removed. Next, the raw data was epoched from -1 to 2.5 seconds relative to trial onset. A visual inspection was carried out to manually remove any non-stereotypical noise from the signals. The baseline was subtracted from the data using the remove epoch baseline method in EEGLAB. Following this, an ICA decomposition was performed using the runica method (Delorme, Sejnowski, & Makeig, 2007; Makeig, Debener, Onton, & Delorme, 2004). Components showing more than 90% probability for eye blink, muscle twitch, and channel noise were flagged for rejection. Additionally, components classified as residual gradient noise were manually removed. Epochs were again visually inspected to further eliminate residual noise before applying EEGLAB epoch rejection methods, which involved rejecting epochs with abnormal values exceeding 50 μV, improbable data with more than 5 standard deviations between channels, and improbable trends with a

maximum slope/epoch of 50. Subsequently, the data was re-epoched from 500 ms prior to the onset of the tone to 1300 ms after the onset of the lane-change. For the single tone condition, data was epoched from 500 ms before the tone onset to 1500 ms after the tone onset. Eventually, signal-to-noise (SNR) ratio was calculated for each participant based on epoched data and participants for which SNR was lower than 3 were rejected. One subject was rejected based on SNR.

Multivariate pattern analysis (MVPA)

To measure temporal dynamics of dual-task information processing, we applied the MVPA analysis method on the EEG data for the lane-change and tone tasks, separately. In each task, three conditions of the short and the long SOAs, and the single task were predefined. In case of the tone discrimination task in each condition MVPA was applied to data to assess whether information about the tone discrimination (high vs low) is encoded differently across conditions (Marti et al., 2015; Rajaei et al., 2019). Likewise, the same procedure was applied to the lane-change task to differentiate left vs right shift in each condition. For each participant and each task, trials of the short and the long SOAs and single conditions were extracted from the EEG data. Then, data was normalized (Z-transformed baseline normalization) by their baseline of 200 to 0 ms prior to the stimulus onset.

Subsequently for each task at each time-point a data matrix of number of all trials x number of sensors was created per condition. We first normalized the matrix (z-score of each channel-time feature) and then used a support vector machine (SVM) with a kernel function using MATLAB “fitcsvm” to decode right vs left in the lane-change task

and high vs low in tone task, with a 10-fold stratified cross validation approach. Stratified means the same proportion of each class was kept within each fold. To compensate for fewer number of trials in single condition and get a reliable comparison we applied a trial matching procedure. First, we randomly drew a set of trials from short and long SOAs with same number of trials of single condition. We proceeded by training and optimizing the classifier using a 10-fold cross-validation approach. This methodology was iterated 100 times, and the results were averaged across the 100 datasets to obtain the trial-matched decoding accuracy.

Time-time decoding analysis

Time-time decoding accuracies were also obtained by cross-decoding across time. Each SVM classifier trained at a given time was tested at all other time-points and then averaged over the 10-fold cross validation, thereby demonstrating the cross-validated generalization across time. The complete ‘‘temporal generalization’’ (King & Dehaene, 2014) resulted in a matrix of training time * testing time.

Generalization across Conditions

To evaluate how brain responses of each task were affected by the dual-task paradigm, the optimized SVM classifier for each condition at any given time was tested on its ability to successfully discriminate classes of each task at all the time samples of other conditions. The process was also executed through cross-validation and subsequently averaged to produce the mean classification accuracy across conditions. The outcome was a training-time by testing-time matrix that was generalized across conditions.

Searchlight analysis

To determine which electrode contributed most to the decoding performance in each time bin, searchlight analysis was used. In this analysis time was the feature matrix and the decoding performance of each electrode neighborhood was calculated. First, the square distance of electrodes was calculated using X and Y position of electrodes. Subsequently, electrodes for which this distance was less than 0.3 were considered neighbors and averaged together. Finally, a sliding window of 50 ms with steps of 4 ms was used and at each step the classification was carried out at the corresponding window. MVPA-light package was used to compute decoding performance with nonlinear SVM as classifier and a 10-fold stratified cross-validation method (Treder, 2020). Similar trial matching method was applied to the short and the long SOA conditions.

Statistical Analyses

For each participant and each task, first the averaged cross-validated accuracy was calculated per condition at each time point. Then, we used the nonparametric Wilcoxon signed-rank test for random effect analysis. To determine time-points with significant above chance accuracy, we used a right-sided signed-rank test across participants (n = 19). To adjust p-values for multiple comparisons (e.g. across time), we further applied the false discovery rate (FDR) correction (FDR $q < 0.05$) (Groppe, 2023). In addition, to determine whether two conditions were significantly different at any time interval, we used a two-sided signed-rank test, FDR corrected across time.

Subsequently, nonparametric effect sizes are reported with an area under the curve (AUC) computed from the receiver operating curves (ROC) for searchlight analysis,

temporal and conditional generalizations. AUC represents relative predictions of true positives (e.g., a trial was correctly classified as left/right in lane-change task or high/low in tone task) and predictions of false positives (e.g., a trial was incorrectly classified). An AUC of 0.5 corresponds to chance level as it means that true positives and false positives are equiprobable. Conversely an AUC of 1 means a perfect prediction of a given class. We used signed-rank tests with a threshold set at alpha = 0.05 to assess whether classifiers could predict the trials' classes above chance level (50%). A correction for multiple comparisons was then applied with a false discovery rate (FDR $q < 0.05$).

One-way repeated measures ANOVA followed by Tukey HSD multiple comparison test was used to compare differences between the conditions for behavioral performance, reaction times and estimated parameters of drift diffusion model. Greenhouse-Geisser correction was performed whenever sphericity had been violated.

Significance testing

For each participant, we measured the onset latency, offset latency and duration of each classification time course. Onset latency: At each training time, onset latency was defined as the earliest time where performance became significantly above chance (i.e., AUC > 0.5) for at least 5 consecutive time bins (20 milliseconds). Mean and standard deviation (SD) for onset latencies were calculated by resampling the data 100 times. In each iteration 19 participants with replacement were chosen from the data and the onset was calculated with the aforementioned definition. Offset latency: Likewise, offset latency for each training time was defined as the earliest time where performance

became non-significant for at least 5 consecutive time bins (20 milliseconds). Mean and SD for offset latencies were also calculated by resampling. Finally, duration was the difference between offset and onset latencies.

Supplemental Information

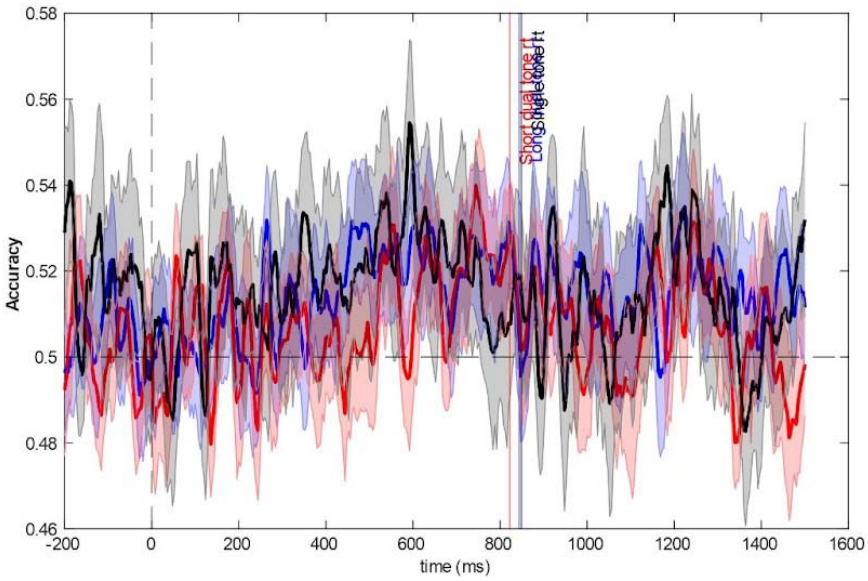

Figure S1. Temporal dynamics of dual task interference in tone task.

For each subject, a nonlinear SVM as a MVPA method was trained in each time bin to discriminate between high vs low in tone task and cross-validated accuracies were calculated and averaged across 19 subjects. As was mentioned, decoding performance of tone task was markedly compromised by the more salient driving task as a result there was no period of significantly above chance performance in neither of the

conditions nor their difference were significant. Shaded error bars represent SEM. Horizontal dashed line represents 50% accuracy corresponding to chance level. The vertical dashed line shows the stimulus (tone) onset. Three vertical lines are the corresponding reaction times of each condition.

References

Abbas-Zadeh, M., Hossein-Zadeh, G.-A., & Vaziri-Pashkam, M. (2021). Dual-task interference in a simulated driving environment: serial or parallel processing? *Frontiers in psychology, 11*, 579876.

Abbaszadeh, M., Hossein-Zadeh, G.-A., Seyed-Allaei, S., & Vaziri-Pashkam, M. (2023). Disturbance of information in superior parietal lobe during dual-task interference in a simulated driving task. *Cortex, 167*, 235-246.

Acerbi, L., & Ma, W. J. (2017). Practical Bayesian optimization for model fitting with Bayesian adaptive direct search. *Advances in neural information processing systems, 30*.

Dale, A., Greve, D., & Burock, M. (1999). Optimal stimulus sequences for event-related fMRI. *NeuroImage, 9*, S33-S33.

Dell'Acqua, R., Jolicoeur, P., Vespignani, F., & Toffanin, P. (2005). Central processing overlap modulates P3 latency. *Experimental Brain Research, 165*, 54-68.

Delorme, A., & Makeig, S. (2004). EEGLAB: an open source toolbox for analysis of single-trial EEG dynamics including independent component analysis. *Journal of neuroscience methods, 134*(1), 9-21.

Delorme, A., Sejnowski, T., & Makeig, S. (2007). Enhanced detection of artifacts in EEG data using higher-order statistics and independent component analysis. *NeuroImage, 34*(4), 1443-1449.

Duncan, J. (1980). The locus of interference in the perception of simultaneous stimuli. *Psychological review, 87*(3), 272.

Gold, J. I., & Shadlen, M. N. (2007). The neural basis of decision making. *Annu. Rev. Neurosci., 30*, 535-574.

Groppe, D. (2023, October 27, 2023.). fdr_bh. *(https://www.mathworks.com/matlabcentral/fileexchange/27418-fdr_bh), MATLAB Central File Exchange. Retrieved October 27, 2023.*

Hibberd, D. L., Jamson, S. L., & Carsten, O. M. (2013). Mitigating the effects of in-vehicle distractions through use of the Psychological Refractory Period paradigm. *Accident Analysis & Prevention, 50*, 1096-1103.

Huestegge, L., & Koch, I. (2010). Crossmodal action selection: Evidence from dual-task compatibility. *Memory & Cognition, 38*, 493-501.

King, J.-R., & Dehaene, S. (2014). Characterizing the dynamics of mental representations: the temporal generalization method. *Trends in cognitive sciences, 18*(4), 203-210.

Levy, J., Pashler, H., & Boer, E. (2006). Central interference in driving: Is there any stopping the psychological refractory period? *Psychological science, 17*(3), 228-235.

Makeig, S., Debener, S., Onton, J., & Delorme, A. (2004). Mining event-related brain dynamics. *Trends in cognitive sciences, 8*(5), 204-210.

Marti, S., King, J.-R., & Dehaene, S. (2015). Time-resolved decoding of two processing chains during dual-task interference. *Neuron, 88*(6), 1297-1307.

Marti, S., Sigman, M., & Dehaene, S. (2012). A shared cortical bottleneck underlying attentional blink and psychological refractory period. *NeuroImage, 59*(3), 2883-2898.

Matthews, A., Garry, M. I., Martin, F., & Summers, J. (2006). Neural correlates of performance trade-offs and dual-task interference in bimanual coordination: an ERP investigation. *Neuroscience letters, 400*(1-2), 172-176.

McCann, R. S., & Johnston, J. C. (1992). Locus of the single-channel bottleneck in dual-task interference. *Journal of Experimental Psychology: Human Perception and Performance, 18*(2), 471.

Pashler, H. (1994). Graded capacity-sharing in dual-task interference? *Journal of Experimental Psychology: Human Perception and Performance, 20*(2), 330.

Pashler, H., & Johnston, J. C. (1989). Chronometric evidence for central postponement in temporally overlapping tasks. *The Quarterly Journal of Experimental Psychology, 41*(1), 19-45.

Pratt, N., Willoughby, A., & Swick, D. (2011). Effects of working memory load on visual selective attention: behavioral and electrophysiological evidence. *Frontiers in human neuroscience, 5*, 57.

Rajaei, K., Mohsenzadeh, Y., Ebrahimpour, R., & Khaligh-Razavi, S.-M. (2019). Beyond core object recognition: Recurrent processes account for object recognition under occlusion. *PLoS computational biology, 15*(5), e1007001.

Ratcliff, R., Smith, P. L., Brown, S. D., & McKoon, G. (2016). Diffusion decision model: Current issues and history. *Trends in cognitive sciences, 20*(4), 260-281.

Raymond, J. E., Shapiro, K. L., & Arnell, K. M. (1992). Temporary suppression of visual processing in an RSVP task: An attentional blink? *Journal of Experimental Psychology: Human Perception and Performance, 18*(3), 849.

Ruthruff, E., Pashler, H. E., & Klaassen, A. (2001). Processing bottlenecks in dual-task performance: structural limitation or strategic postponement? *Psychonomic bulletin & review, 8*(1), 73-80.

Shadlen, M. N., & Newsome, W. T. (2001). Neural basis of a perceptual decision in the parietal cortex (area LIP) of the rhesus monkey. *Journal of neurophysiology, 86*(4), 1916-1936.

Shinn, M., Lam, N. H., & Murray, J. D. (2020). A flexible framework for simulating and fitting generalized drift-diffusion models. *ELife, 9*, e56938.

Sigman, M., & Dehaene, S. (2005). Parsing a cognitive task: a characterization of the mind's bottleneck. *PLoS biology, 3*(2), e37.

Sigman, M., & Dehaene, S. (2006). Dynamics of the central bottleneck: Dual-task and task uncertainty. *PLoS biology, 4*(7), e220.

Sigman, M., & Dehaene, S. (2008). Brain mechanisms of serial and parallel processing during dual-task performance. *Journal of Neuroscience, 28*(30), 7585-7598.

Sternberg, S. (1969). The discovery of processing stages: Extensions of Donders' method. *Acta psychologica, 30*, 276-315.

Strayer, D. L., & Johnston, W. A. (2001). Driven to distraction: Dual-task studies of simulated driving and conversing on a cellular telephone. *Psychological science, 12*(6), 462-466.

Töllner, T., Strobach, T., Schubert, T., & Mueller, H. (2012). The effect of task order predictability in audio-visual dual task performance: Just a central capacity limitation? *Frontiers in Integrative Neuroscience, 6*. doi:10.3389/fnint.2012.00075

Tombu, M., & Jolicœur, P. (2002). All-or-none bottleneck versus capacity sharing accounts of the psychological refractory period phenomenon. *Psychological research, 66*, 274-286.

Tombu, M., & Jolicœur, P. (2003). A central capacity sharing model of dual-task performance. *Journal of Experimental Psychology: Human Perception and Performance, 29*(1), 3.

Tombu, M. N., Asplund, C. L., Dux, P. E., Godwin, D., Martin, J. W., & Marois, R. (2011). A unified attentional bottleneck in the human brain. *Proceedings of the National Academy of Sciences, 108*(33), 13426-13431.

Treder, M. S. (2020). MVPA-light: a classification and regression toolbox for multi-dimensional data. *Frontiers in Neuroscience, 14*, 289.

Voss, A., Voss, J., & Lerche, V. (2015). Assessing cognitive processes with diffusion model analyses: A tutorial based on fast-dm-30. *Frontiers in psychology, 6*, 336.

Welford, A. T. (1952). The psychological refractory period and the timing of high-speed performance-a review and a theory. *British Journal of Psychology, 43*(1), 2.

Zylberberg, A., Ouellette, B., Sigman, M., & Roelfsema, P. R. (2012). Decision making during the psychological refractory period. *Current biology, 22*(19), 1795-1799.